Anticancer Activity of Reconstituted Ribonuclease S-Decorated Artificial Viral Capsid

Yingbing Liang,[a] Hiroto Furukawa,[a] Kentarou Sakamoto,[a] Hiroshi Inaba,[a, b] and Kazunori Matsuura*[a, b]

Ribonuclease S (RNase S) is an enzyme that exhibits anticancer activity by degrading RNAs within cancer cells; however, the cellular uptake efficiency is low due to its small molecular size. Here we generated RNase S-decorated artificial viral capsids with a size of 70–170 nm by self-assembly of the β-annulus-S-peptide followed by reconstitution with S-protein at neutral pH.

The RNase S-decorated artificial viral capsids are efficiently taken up by HepG2 cells and exhibit higher RNA degradation activity in cells compared with RNase S alone. Cell viability assays revealed that RNase S-decorated capsids have high anticancer activity comparable to that of standard anticancer drugs.

Introduction

Ribonuclease (RNase)[1] is an enzyme that degrades ribonucleic acid into oligonucleotides and mononucleotides, which is attracting attention as an enzyme preparation that exhibits anticancer activity by administering into cancer cells.[2–15] When RNase is administered to cancer cells, it exhibits anticancer effects by degrading intracellular ribonucleic acid, inducing apoptosis by caspases, proteolytic enzymes involved in programmed cell death, and regulating DNA transcription, and cytokine production.[16,17] Since cancer cells have specific ligands for RNase on their surface, RNases selectively accumulate into cancer cells.[2,18] In addition, RNase are not toxic for normal cells grown *in vitro*, nor does it exert appreciable toxic effects when administered *in vivo* to experimental animals.[2,18] Thus, many attempts to use RNase as anticancer enzyme drugs have been reported. For example, D'Alessio et al. reported that treatment of tumor cells with bovine seminal RNase resulted in the suppression of intracellular protein synthesis by rRNA degradation and antitumor activity.[14] Magun et al. succeeded in inducing cell death by introducing the amphibian cytotoxic RNase, Onconase, into cancer cells.[15]

With respect to enzyme replacement therapy, small-sized enzymes are introduced into cells, but penetration into specific cells and tissues may be limited.[19] The cellular uptake efficiency of nanoparticles depends on the size, and particles of approximately 50 nm are efficiently taken up.[20,21] RNase alone exhibits low uptake efficiency in cells due to its small molecular size (typically 3–4 nm); therefore, excess amounts of RNase must be added in vitro or in vivo to achieve a high uptake efficiency. However, an overdose of RNase may occur resulting in high cytotoxicity to cells other than cancer cells.[22]

Naturally occurring spherical viruses have a size of typically 30–50 nm.[23] They may be exploited as a carrier for forming complexes with enzymes to increase the cellular uptake efficiency of enzymes. Spherical viral capsids consist of protein shells with an icosahedral symmetry and have been used for encapsulating enzymes in place of viral nucleic acids.[24–27] In addition, viral capsids decorated on the surface with enzymes can enhance cellular uptake.[28–31] For example, Jaimes et al. decorated the surface of primate erythroparvovirus capsid with α-glucosidase.[30] Evans et al. constructed a cowpea mosaic virus capsid decorated with horseradish peroxidase and glucose oxidase, which exhibited high enzymatic activity.[31] Although natural and mutated viral capsids have been used as enzyme carriers, diverse molecular designs that may impart arbitrary functions are limited.
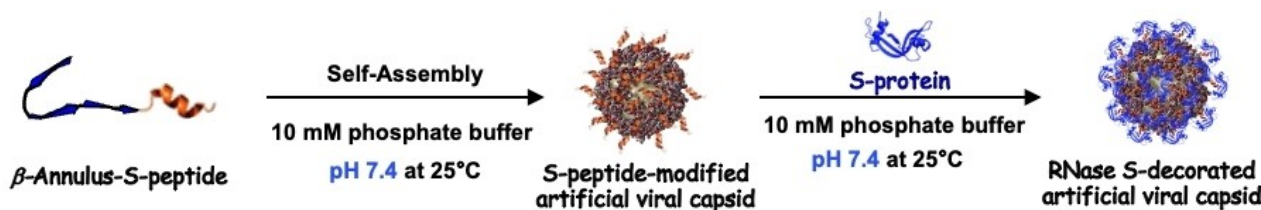
Recently, viral capsid-like nanocapsules that self-assemble from artificially designed proteins or peptides have been created that possess various functions.[32–47] The artificial design of symmetric assembling protein subunits has enabled the construction of protein nanocages that exhibit cubic, dodecahedral, and icosahedral symmetry.[45–47] We established an artificial viral capsid with a diameter of 30–50 nm self-assembled from a 24-residue peptide (INHVGGTGGAIMAPVAVTRQLVGS) of β-annulus motif, which is involved the formation of the endoskeleton of tomato bushy stunt virus.[48–50] The N-terminus of the β-annulus peptide is directed inside the capsid, which facilitates the encapsulation of DNA,[51,52] mRNA[53] or His-tagged GFP[54,55] in the artificial viral capsid. Since the C-terminus is directed to the outside of the capsid, gold nanoparticles[56] and proteins[57,58] were decorated on the surface of the capsids.

[a] Y. Liang, H. Furukawa, Dr. K. Sakamoto, Dr. H. Inaba, Prof. Dr. K. Matsuura
Department of Chemistry and Biotechnology
Graduate School of Engineering, Tottori University
Koyama-Minami 4–101, Tottori
680-8552 (Japan)
E-mail: ma2ra-k@tottori-u.ac.jp
[b] Dr. H. Inaba, Prof. Dr. K. Matsuura
Centre for Research on Green Sustainable Chemistry
Tottori University, Koyama-Minami 4–101,
Tottori 680-8552 (Japan)

ChemBioChem

Research Article
doi.org/10.1002/cbic.202200220

**Chemistry
Europe**
European Chemical
Societies Publishing

Scheme 1. Schematic illustration of construction of RNase S-decorated artificial viral capsid in 10 mM phosphate buffer (pH 7.4).

The split enzyme, RNase S, is reconstituted from S-protein and S-peptide, which are produced by digesting RNase A with subtilisin.[1] The ease of association (the association constant: 7×10^6 M^{-1} at 25 °C) has been used as a reversible component of enzymatic supramolecular assemblies.[59–66] We successfully created an artificial viral capsid decorated with RNase S by reconstructing the S-protein on the surface of an S-peptide-modified artificial viral capsid.[67] However, the assembly was done using an acetic acid buffer (pH 4.5), which is not suitable for studies evaluating anticancer activity in cultured cells. In this study, we constructed an RNase S-decorated artificial viral capsid in phosphate buffer at pH 7.4 and evaluated the assembled structure, uptake into cancer cells, degradation of intracellular RNA, and anticancer effects.

Results and Discussion

Based on our previous report,[67] β-annulus-S-peptide was prepared by native chemical ligation of benzylthioesterified β-annulus peptide at the C-terminus (β-annulus-SBn: IN-HVGGTGGAIMAPVAVTRQLVGG-*SBn*, Figure S1) with the S-peptide containing Cys at the N-terminus (Cys-S-peptide: CGGGKE-TAAAKFERQHMDS). The β-annulus-S-peptide was purified by reversed-phase HPLC and confirmed by MALDI-TOF-MS (Figure S2). We previously explored how to construct an RNase S-decorated artificial viral capsid with enzymatic activity by the self-assembly of β-annulus-S-peptide followed by the reconstruction with the S-protein.[67] Although the self-assembly of β-annulus-S-peptide was attempted in neutral water adjusted with NaOH and in Tris-HCl buffer (pH 7.4), the β-annulus-S-peptide formed aggregates not spherical structures with the size of about 50 nm. Unavoidably, we allowed the β-annulus-S-peptide to self-assemble at pH 4.5 to construct RNase S-decorated artificial viral capsid. Since these conditions are not suitable for cellular experiments, we reexamined the conditions for the self-assembly the β-annulus-S-peptide. By dissolving the β-annulus-S-peptide in phosphate buffer at pH 7.4 followed by sonication, we succeeded in constructing S-peptide-modified and RNase S-decorated artificial viral capsids (Scheme 1).The synthesized β-annulus-S-peptide was dissolved by sonication for 30 s in phosphate buffer at pH 7.4 and incubated at 25 °C for 40 min to allow self-assembly. The size distribution obtained from dynamic light scattering (DLS) measurement of the solution of β-annulus-S-peptide (25 μM) at pH 7.4 was 47 ± 23 nm (Figure S3), which was similar to that at pH 4.5. This

indicates that the S-peptide-modified artificial viral capsid may be constructed at neutral pH.

The RNase S-decorated capsid was constructed by incubating an equimolar (25 μM) mixture of the S-peptide- modified capsid and S-protein at 25 °C for 4 h in phosphate buffer (pH 7.4). The reconstruction of RNase S on the surface of the capsid was confirmed by CD spectra as it is known that the ellipticity increases more negatively around 215–235 nm by the reconstruction of RNase S compared with the S-protein alone.[68] The negative molar ellipticity of the S-protein was increased by forming a complex with equimolar β-annulus-S-peptide in phosphate buffer (Figure 1). This suggests that the reconstitution of RNase S on the surface of the capsid may be achieved at pH 7.4. This increase in the negative ellipticity was a large change compared with that in acetate buffer (pH 4.5).[67] Therefore, it appears that more RNase S may be reconstituted at pH 7.4 with a secondary structure containing a higher α-helix content compared with that at pH 4.5.

The DLS of the aqueous solution of RNase S-decorated capsid reconstituted at pH 7.4 showed the formation of an assembly with a size of 71 ± 43 nm (Figure 2A). The increase in particle size compared with the S-peptide-modified capsid (Figure S3) was probably caused by reconstruction of RNase S on the capsid. In Transmission electron microscopy (TEM) images, hollow spherical structures with a rugged wall were evident, but the particle size was approximately 100–170 nm (Figure 2B). In contrast, TEM images of the S-peptide modified
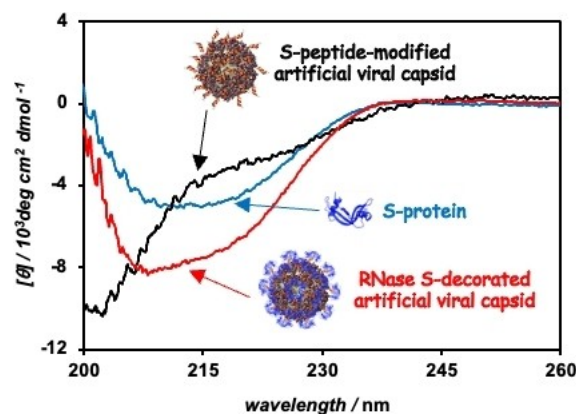

Figure 1. CD spectra of S-peptide-modified artificial viral capsid ([β-annulus-S-peptide] = 25 μM, black), 25 μM S-protein (blue), and RNase S-decorated artificial viral capsid ([β-annulus-S-peptide] = [S-protein] = 25 μM, red) in 10 mM phosphate buffer (pH 7.4) at 25 °C.
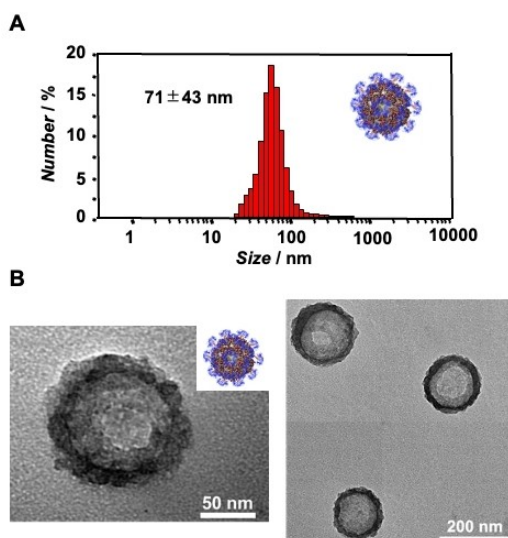
Figure 2. (A) Size distribution obtained from DLS and (B) TEM images of RNase S-decorated artificial viral capsid ([β-annulus-S-peptide] = [S-protein] = 25 μM) in phosphate buffer (pH 7.4) at 25 °C.

capsid showed spherical structures with a size of 70–150 nm (Figure S4), which is smaller than that of RNase S decorated capsid observed by TEM. These results support the decoration of RNase S on the capsids.

Under drying conditions for TEM observation, the spherical capsid became deformed to a spheroid and the observed particle size appeared larger. The enzymatic activity of the RNase S-decorated capsid was evaluated using the RNaseAlert® Lab Test Kit (Thermo Fisher Scientific) in which fluorescence intensity of the RNA substrate was enhanced by cleaving the RNA strand with ribonuclease. The RNase S-decorated capsid retained approximately 85% of its original enzymatic activity compared with RNase S alone at pH 7.4 (Figure 3), which was similar to the result at pH 4.5.[67] The activity of RNase S-decorated capsid was kept approximately 81% enzyme activity
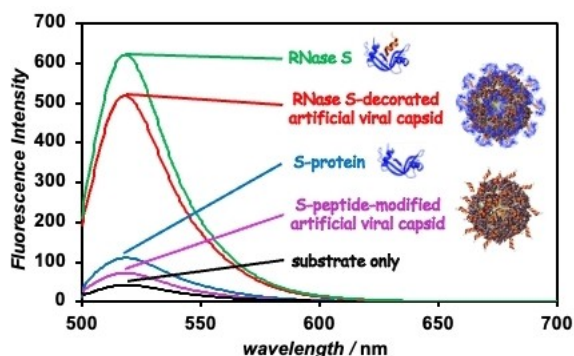

Figure 3. Fluorescence spectra of the reaction mixtures using the RNaseAlert Lab Test in the presence of 25 μM RNase S (green), RNase S-decorated artificial viral capsid ([β-annulus-S-peptide] = [S-protein] = 25 μM, red), 25 μM S-protein (blue), S-peptide-modified artificial viral capsid ([β-annulus-S-peptide] = 25 μM, purple), and substrate only (black) in 10 mM phosphate buffer (pH 7.4) at 25 °C. The excitation wavelength was 490 nm.

of RNase S alone even after 24 hours of incubation in DMEM medium (Figure S5), indicating that the RNase S decorated capsid is sufficiently stable in physiological condition.

Since the RNase S-decorated artificial viral capsid exhibits high enzymatic activity, the capsid was predicted to show anticancer activity. The uptake of the RNase S-decorated capsid into human hepatoma HepG2 cells was evaluated by confocal laser scanning microscopy (CLSM). A RNase S-decorated fluorescent tetramethylrhodamine (TMR)-labeled capsid was constructed by co-assembling TMR-β-annulus and β-annulus-S-peptide (Figure S6). As a control, TMR-RNase S was prepared by reconstituting TMR-labeled S-peptide with S-protein (Figure S7). Following the addition of the TMR-labeled capsid to HepG2 cells, the cells were cultured at 37 °C in 5% CO_2 for 48 h. The CLSM images revealed that more red fluorescence was evident in cells by adding RNase S-decorated TMR-labeled capsid compared with TMR-RNase S (Figure 4A,B, S8). The quantified intracellular TMR-fluorescence distribution showed a significant difference between TMR-RNase S and RNase S-decorated TMR-labeled capsid (Figure 4C, $p < 0.001$***). These results indicate that the cellular uptake efficiency of RNase S-decorated capsid with a size of approximately 100 nm was higher compared with RNase S alone.

To evaluate whether the intracellular RNA is degraded by RNase S-decorated capsids, HepG2 cells were stained with Strand Brite ™ RNA Green (AAT Bioquest, Inc.), which fluoresces upon binding to intracellular RNA (Figure 5A). The CLSM images RNAs decreased following the addition of TMR-RNase S alone or RNase S-decorated TMR-labeled capsid compared with un-
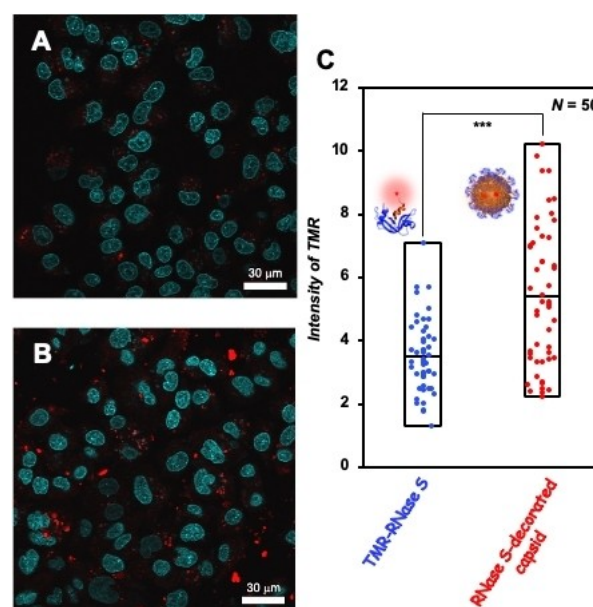
Figure 4. Cellular uptake of RNase S-decorated artificial viral capsid. Confocal laser scanning microscopy (CLSM) images of HepG2 cells in the presence of (A) TMR-labeled RNase S ([S-protein] = [TMR–S-peptide] = 25 μM) and (B) TMR-labeled RNase S-decorated artificial viral capsid ([S-protein] = [S-protein] = 25 μM, [TMR-β-annulus] = 5 μM). (C) Box plot of the fluorescence intensity distribution of TMR ($N = 50$). ***, $p < 0.001$ by a one-way analysis of variance (ANOVA) followed by Mann-Whitney U test.

ChemBioChem

Research Article
doi.org/10.1002/cbic.202200220

Chemistry
Europe
European Chemical
Societies Publishing

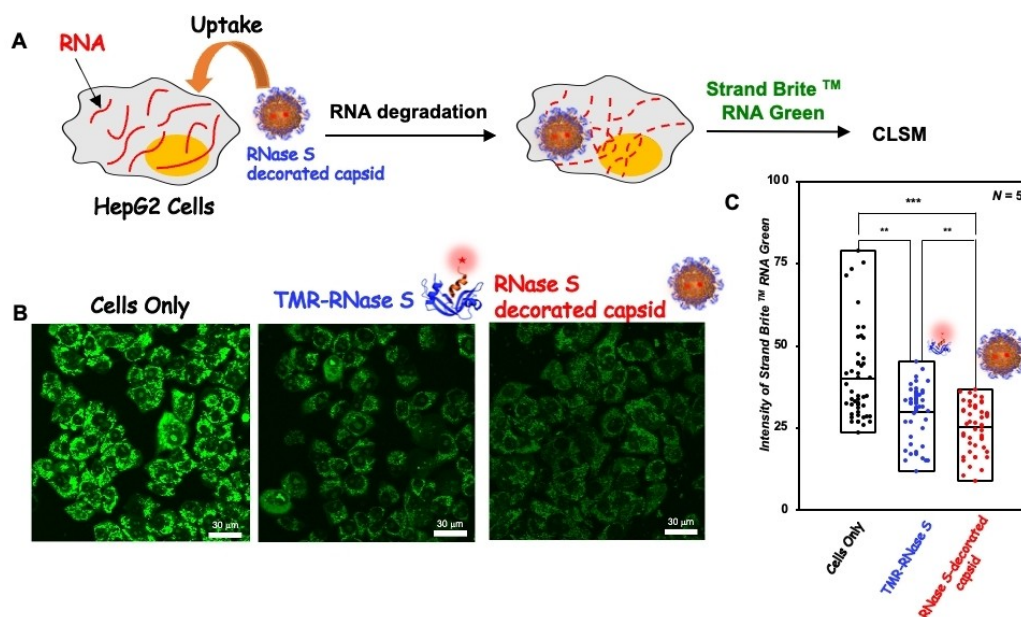**Figure 5.** (A) Schematic illustration of HepG2 cell RNA degradation by RNase S-decorated artificial viral capsid. (B) CLSM images of HepG2 cells in the absence and presence of 25 μM RNase S or RNase S-decorated artificial viral capsid ([β-annulus-S-peptide] = [S-protein] = 25 μM). Channel for Strand Brite ™ RNA Green (green). (C) Box plot of the fluorescence intensity distribution of Strand Brite ™ RNA green (N = 50). ***, p < 0.001, **, p < 0.01, by a one-way ANOVA followed by Kruskal–Wallis test.

treated cells (Figure 5B). Quantitative analysis revealed that the green fluorescence intensity inside the cells was decreased in the following order: untreated cells > TMR-RNase S > RNase S-decorated TMR-labeled capsid (Figure 5C). These results indicate that the RNase S-decorated TMR-labeled artificial viral capsid was successfully introduced into HepG2 cells and degraded the intracellular RNA; however, the intracellular RNA-derived fluorescence did not completely disappear by the RNase S-decorated capsid. This may be the result of incomplete escape of the capsid from the endosomes.

To estimate the extent of RNA degradation by the RNase S-decorated capsid in HepG2 cells, the intracellular RNAs were extracted and quantified. After addition of each sample to the cells and incubating for 48 h at 37 °C and 5% CO_2, the RNAs were extracted and quantified. Following the addition of RNase S-decorated capsid ([β-annulus-S-peptide] = [S-protein] = 25 μM), the amount of RNA in HepG2 cells was decreased to 56% of the original amount (Figure 6A). In contrast, the addition of S-peptide-modified capsid and S-protein alone minimally affected the intracellular RNA quantity. Interestingly, RNase S-decorated capsid resulted in more RNA degradation compared with RNase S or RNase A alone at the same concentration (25 μM), probably as a result of higher cellular uptake. Figure 6B shows the time course of the amount of intracellular RNA by the addition of RNase S-decorated capsid and actinomycin D (1.9 μM), which is a commercial anticancer drug that inhibits intracellular RNA synthesis.[69] The rate of decrease of RNA by the addition of RNase S-decorated capsid was slower compared with that following the addition of actinomycin D, although both had similar amounts of RNA after 48 h. Since actinomycin D is an anticancer drug that inhibits the

synthesis of RNA in cancer cells, the amount of RNA decreased relatively rapidly, whereas RNase S-decorated capsid gradually degraded intracellular RNA.

Finally, the anticancer activity of RNase S-decorated capsid was evaluated using a water-soluble tetrazolium salt (WST) assay, a method for measuring cell viability. It is known that WST-8 is reduced to a water-soluble formazan by lactate dehydrogenase in living cells, which exhibits increased absorbance at 450 nm.[70] After each sample was added to HepG2 cells and incubated at 37 °C and 5% CO_2 for 48 h, the absorbance at 450 nm was measured (Figure 7A). By adding an RNase S-decorated artificial viral capsid ([β-annulus-S-peptide] = [S-protein] = 25 μM), cell viability was decreased by 52% of the untreated cells, which is comparable to that of the commercial anticancer drugs, taxol and actinomycin D (Figure 7B). RNase S-decorated capsid exhibited a lower cell viability compared with RNase S or RNase A alone at the same concentration. The higher anticancer activity may be caused by higher intracellular uptake efficiency (Figure 4) and intracellular RNA degradation activity (Figures 5, 6) of the RNase S-decorated artificial viral capsid.

Conclusion

We successfully constructed an RNase S-decorated artificial viral capsid that exhibited enzyme activity by reconstituting β-annulus-S-peptide with S-protein in phosphate buffer at pH 7.4. DLS and TEM revealed the formation of hollow spherical structures with a rugged wall and a size of 70–170 nm. We showed that the RNase S-decorated artificial viral capsid could
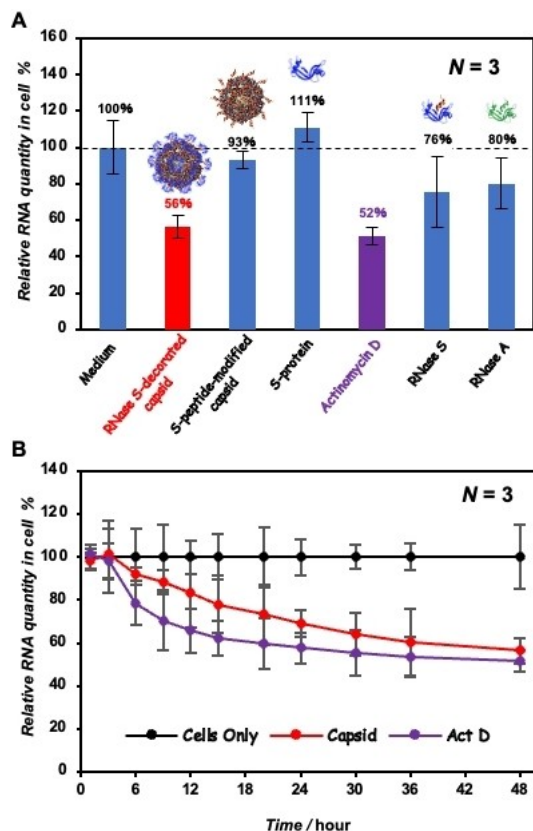
Figure 6. (A) Relative RNA quantity extracted from HepG2 cells after incubation in the presence of each sample for 48 h at 37 °C under 5 % CO_2. RNase S-decorated artificial viral capsid ([β-annulus-S-peptide] = [S-protein] = 25 μM), S-peptide-modified artificial viral capsid ([β-annulus-S-peptide] = 25 μM), 25 μM S-protein, 1.9 μM actinomycin D, 25 μM RNase S, and 25 μM RNase A. (B) Time course of the decrease in RNA in HepG2 cells by the addition of RNase S-decorated capsid ([β-annulus-S-peptide] = [S-protein] = 25 μM) or 1.9 μM actinomycin D (Act D). Results are shown as mean ± standard deviation ($N = 3$).
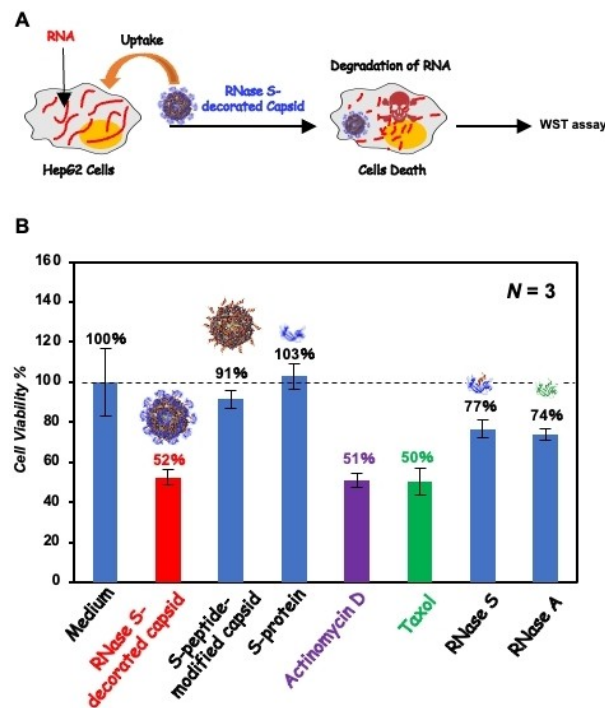
Figure 7. (A) Schematic illustration of the cell viability assay (WST assay). (B) Cytotoxicity of HepG2 cells incubated in the presence of each sample for 48 h at 37 °C under 5 % CO_2. RNase S-decorated artificial viral capsid ([β-annulus-S-peptide] = [S-protein] = 25 μM), S-peptide-modified artificial viral capsid ([β-annulus-S-peptide] = 25 μM), 25 μM S-protein, 1.9 μM actinomycin D, 25 μM taxol, 25 μM RNase S, and 25 μM RNase A.

be introduced into HepG2 cells more efficiently than RNase S alone and sufficiently degraded intracellular RNAs. Furthermore, RNase S-decorated capsids exhibited anticancer activity comparable with anticancer drugs due to higher cell uptake and intracellular RNA degradation. Although the present study focused on the anticancer activity of the RNase S-decorated artificial viral capsid at the cellular level as a first step in the proof of concept, the anticancer experiments *in vivo* level would enhance the impact and practicality of this molecular system. In near future, we plan to analyze the pharmacokinetics of the RNase S-decorated artificial viral capsids in mice and the anticancer activity in more detail. The molecular strategy of enzyme-decorated artificial viral capsids provides a new perspective for enzyme replacement therapy and anticancer drug research.

Experimental Section

General methods: Reversed-phase HPLC was performed at ambient temperature using a Shimadzu LC-6AD liquid chromatography system equipped with a UV/vis detector (220 nm, Shimadzu SPD-10AVvp) and Inertsil ODS-3 or WP300 C4 (GL Science) columns (250 × 4.6 mm or 250 × 20 mm). MALDI-TOF mass spectra were obtained using an Autoflex T2 instrument (Bruker Daltonics) in linear/positive mode with α-cyano-4-hydroxy cinnamic acid (α-CHCA) as the matrix. CD spectra were measured at 25 °C in a 1.0 mm quartz cell using a JASCO J-820 spectrophotometer equipped with a Peltier-type thermostatic cell holder. Ribonuclease S from bovine pancreas was purchased from Sigma-Aldrich and separated into the S-peptide and S-protein fractions using reversed-phase HPLC with a Inertsil WP300C4 (GL Science) column according to the literature.[66] Other reagents were obtained from commercial sources and were used without further purification. Ultrapure water of high resistivity (> 18 MΩ cm) was purified using a Millipore Purification System (Milli-Q water) and was used as a solvent for the peptides. Ultrapure™ DNase/RNase-Free Distilled Water was purchased from Thermo (500 mL, Thermo Fisher Scientific).

Synthesis of β-annulus-S-peptide: The β-annulus-S-peptide (INHVGGTGGAIMAPVAVTRQLVGGCGGGKETAAAKFERQHMDS) was synthesized by native chemical ligation of benzylthioesterified β-annulus peptide at the C-terminus (β-annulus-SBn: INHVGGTGGAIM APVAVTRQLVGG-SBn) with S-peptide bearing Cys at the N-terminus (Cys-S-peptide: CGGGKETAAAKFERQHMDS) according to our previous report.[67] The peptide was purified by reversed-phase HPLC and confirmed by MALDI-TOF-MS (matrix: α-CHCA, m/z = 4280 [M]$^+$).

Synthesis of TMR-β-annulus peptide: β-Annulus peptide bearing Cys at the N-terminus (CINHVGGTGGAIMAPVAVTRQLVGS) was synthesized on Fmoc-Ser(tBu)-Alko-PEG resin (400 mg, 0.1 mmol/g;

ChemBioChem

Research Article
doi.org/10.1002/cbic.202200220

**Chemistry
Europe**
European Chemical
Societies Publishing

Watanabe Chemical Ind. Ltd.) using Fmoc-based coupling reactions (four equivalents of Fmoc amino acids). An N-methylpyrrolidone (NMP) solution containing (1-cyano-2-ethoxy-2-oxoethylidenami-nooxy) dimethylamino-morpholino-carbenium hexafluorophosphate (COMU) and diisopropylamine was used as the coupling reagent. Fmoc deprotection was achieved using 20% piperidine in N,N-dimethylformamide (DMF). The progression of the coupling reaction and Fmoc deprotection was confirmed by TNBS and a chloranil test kit. Peptidyl resins were washed with NMP and dried under a vacuum. Peptides were deprotected and cleaved from the resin by treatment with a cocktail of trifluoroacetic acid/1,2-ethanedithiol/ triisopropylsilane/thioanisole/water at a 8.25/0.25/0.1/0.5/0.5 (mL) ratio at room temperature for 4 h. Reaction mixtures were filtered to remove resins and the filtrates were concentrated under vacuum. The crude product was purified by reversed-phase HPLC eluting with a linear gradient of CH_3CN/water containing 0.1% TFA (5/95 to 100/0 over 100 min). The fraction containing the desired peptide was lyophilized to give 6.1 mg of a flocculent solid (35% yield) and validated by MALDI-TOF MS (matrix: α-CHCA): $m/z = 2411\ [M+2]^+$. The obtained Cys-β-annulus peptide powder was dissolved in 0.2 mM sodium phosphate buffer (2.93 mL, pH 7.0) in an Eppendorf tube. Then, 100 mM Tris(2-carboxyethyl) phosphine hydrochloride (TCEP-HCl) in water (30 μL) and 10 mM tetramethylrhodamine-5-maleimide (TMR-maleimide, Funakoshi Co., Ltd.) in dimethyl sulfoxide (24 μL) were added to the solution, and the mixture was incubated in the dark at 25 °C for 6 h (final concentration: 20 μM Cys-β-annulus peptide, 1 mM TCEP-HCl, 80 μM TMR-maleimide). After dialysis (Spectra/por7, cutoff Mw 1,000, Spectrum Laboratories, Inc.) in water for 20 h, the sample was purified by reversed-phase HPLC eluting with a linear gradient of CH_3CN/water containing 0.1% TFA (5/95 to 100/0 over 100 min). The fraction containing the desired peptide was lyophilized and dissolved in water (675 μL) to give an aqueous solution of 25 μM TAMRA-β-annulus (28.2% yield), which was subjected to MALDI-TOF MS (matrix: α-CHCA: $m/z = 2893\ [M+2]^+$.

Preparation of TMR-RNase S: The Cys-S-peptide (CGGGKETAAAK-FERQHMDS) was dissolved in 0.2 mM sodium phosphate buffer (2.93 mL, pH 7.0), and then 100 mM TCEP-HCl in water (30 μL) and 10 mM TMR-maleimide in DMSO (24 μL) were added. The mixture was incubated in the dark at 25 °C for 6 h (final concentration: 20 μM Cys-S-peptide, 1 mM TCEP-HCl, 80 μM TMR-maleimide). The obtained TMR–S-peptide was purified by reversed-phase HPLC eluting with a linear gradient of CH_3CN/water containing 0.1% TFA (5/95 to 100/0 over 100 min). The fraction containing TMR–S-peptide was lyophilized (40.1% yield). The formation of TMR–S-peptide was confirmed by MALDI-TOF-MS (matrix: α-CHCA, $m/z = 2507\ [M+2]^+$). The TMR-RNase S was prepared by incubating an equimolar (25 μM) mixture of the TMR–S-peptide and S-protein at 25 °C for 24 h and confirmed by MALDI-TOF-MS (matrix: sinapinic acid, $m/z = 14040\ [M+2]^+$).

Dynamic light scattering (DLS): Stock solutions (0.1 mM) of β-annulus-S-peptide were prepared by dissolution in 10 mM phosphate buffer (pH 7.4) followed by sonication for 30 s. The samples were prepared by diluting stock solutions with 10 mM phosphate buffer (pH 7.4) or mixing with S-protein in the same buffer and were incubated at 25 °C for 40 min. DLS measurements were carried out using a Zetasizer Nano ZS (MALVERN) instrument with an incident He–Ne laser (633 nm) at 25 °C. Correlation times of the scattered light intensities $G(\tau)$ were measured several times, and the means were calculated for the diffusion coefficient. Hydrodynamic diameters of the scattering particles were calculated by the Stokes-Einstein equation.

Transmission electron microscopy (TEM): Aliquots (3 μL) of the DLS samples were applied to hydrophilized carbon-coated Cu-grids (C-SMART Hydrophilic TEM grids, ALLANCE Biosystems) for 1 min

and then removed using filter paper. Subsequently, the TEM grids were instilled in staining solution, 2% phosphotungstic acid $[Na_3(PW_{12}O_{40})\ (H_2O)_n]$ (3 μL), for 1 min and then removed using filter paper. After the sample-loaded carbon-coated grids were dried in vacuo, they were analyzed by TEM (JEOL JEM 1400 Plus) using an accelerating voltage of 80 kV.

Ribonuclease activity assay: The ribonuclease activity of RNase S-decorated artificial viral capsid was measured by fluorescence spectroscopy using the RNaseAlert Lab Test Kit (Thermo Fisher Scientific). A solution of fluorescent RNA substrate in 10× RNaseAlert Lab Test buffer (5 μL) was added to a solution of β-annulus-S-peptide (25 μM) and S-protein (25 μM) in 10 mM phosphate buffer (pH 7.4) and the mixture was vortexed. After incubation at 37 °C for 1 h, the mixture was diluted with 10 mM phosphate buffer (150 μL). When cultured in medium, each sample was added to a mixture of 25% 10 mM phosphate buffer (pH 7.4) and 75% DMEM medium (+10% fetal bovine serum (FBS)) and the mixture was vortexed. After incubation at 37 °C for 1 h and 24 h, the samples were diluted with a mixture of medium and phosphate buffer (150 μL). The fluorescence spectrum of the mixture was measured using a JASCO FP-8200 spectrofluorometer at 25 °C at an excitation wavelength of 490 nm.

HepG2 cell culture: Human hepatoma HepG2 cells were purchased from the RIKEN BioResource Research Center (Ibaraki, Japan) and cultured in Dulbecco's Modified Eagle's Medium (DMEM). All medium contained 10% FBS (v/v), Penicillin-Streptomycin-Neo-mycin (PSN) Antibiotic Mixture (Gibco), 1 mM sodium pyruvate, and 1% MEM nonessential amino acids (v/v, Sigma M7145). Cells were maintained at 37 °C in a 5% CO_2 incubator, and a subculture was performed every 3–4 days.

Intracellular introduction of RNase S-decorated TMR-labeled capsid: HepG2 cells were seeded into a single-well glass bottom dish at 2.0×10^4 cells/well in a final volume of 100 μL and incubated for 24 h at 37 °C and 5% CO_2. Aqueous solutions (25 μL) of capsid co-assembled from RNase S-decorated β-annulus-S-peptide (100 μM)/TMR-β-annulus peptide (20 μM) and TMR-RNase S (100 μM) were dissolved in DMEM (+10% FBS, 75 μL), respectively, and were added to the cells and incubated for 48 h at 37 °C and 5% CO_2. After removal of the solution, 10 μg/mL Hoechst 33342 (100 μL) was added to the cells and incubated for 10 min at 37 °C and 5% CO_2. After washing with PBS, the medium was added to the cells and CLSM measurement (FluoView FV10i, Olympus) was performed. TMR was excited at 553 nm and observed through a 577 nm emission band-pass filter (red). Using the ImageJ analysis software, the average fluorescence intensity per area in the intracellular and extracellular regions were calculated, respectively. By subtracting the extracellular intensity from the intracellular intensity, the background-corrected intracellular fluorescence intensity was quantified. 50 data of fluorescence intensities of TMR for each sample ($N = 50$) were collected and statistically processed. we analyzed the fluorescence intensity of TMR for each sample ($N = 50$).

Fluorescent Imaging of intracellular RNAs: HepG2 cells were seeded onto a single-well glass bottom dish at 2.0×10^4 cells/well in a final volume of 100 μL and incubated for 24 h at 37 °C, 5% CO_2. Aqueous solutions (25 μL) of capsid co-assembled from RNase S-decorated β-annulus-S-peptide (100 μM)/TMR-β-annulus peptide (20 μM) and TMR-RNase S (100 μM) were dissolved in DMEM (+10% FBS, 75 μL), respectively, and then added to the cells and incubated for 48 h at 37 °C in 5% CO_2. Then, the cells were fixed with pure methanol (Fujifilm Co., Ltd.) for 1 min at room temperature and washed with PBS. The cells were immersed in 1% Triton X-100 (Nacalai Tesque Inc.) for 2 min and then washed twice with PBS. Next, the solution was replaced with Strand Brite RNA Green

ChemBioChem

Research Article
doi.org/10.1002/cbic.202200220

Chemistry
Europe
European Chemical
Societies Publishing

(Former ABD Bio quest, Inc.) (0.25 μL, 400× in DMSO) in DMEM (+ 10% FBS, 99.75 μL) and then incubated for 30 min at 37 °C and 5% CO_2. After washing with PBS, the medium was added to the cells and CLSM measurement was performed. Strand Brite RNA Green was excited at 495 nm and observed through a 519 nm emission band-pass filter (green). Using ImageJ analysis software, we analyzed the fluorescence intensity of Strand Brite RNA Green from each sample ($N=50$).

Cell viability assay (WST assay): The cultured HepG2 cells were plated in 96-well plates at a density of 1.0×10^4 cells/well in a final volume of 100 μL and incubated for 24 h at 37 °C and 5% CO_2. The culture medium was replaced with medium containing RNase S-decorated capsid ([β-annulus-S-peptide] = [S-protein] = 25 μM), S-peptide-modified artificial viral capsid ([β-annulus-S-peptide] = 25 μM), 25 μM S-protein, 25 μM taxol, 1.9 μM actinomycin D, 25 μM RNase S, or 25 μM RNase A and then incubated for 48 h at 37 °C and 5% CO_2. The culture medium was replaced with fresh medium (100 μL), and Cell Counting Kit-8 reaction solution (10 μL, Dojindo, Japan) was added to each well. After incubating for 4 h, the absorbance at 450 nm was measured using a NanoDrop™ One/OneC (ND-ONE–W, Thermo Fisher Scientific). Cell viability (%) was calculated by setting the absorbance of the untreated control cells at 100%.

Extraction and quantification of RNA in HepG2 cells: The cultured HepG2 cells were seeded into 96-well plates at 1.0×10^4 cells/well in a final volume of 100 μL and incubated for 24 h at 37 °C and 5% CO_2. The culture medium was replaced with medium containing RNase S-decorated capsid ([β-annulus-S-peptide] = [S-protein] = 25 μM), S-peptide-modified artificial viral capsid ([β-annulus-S-peptide] = 25 μM), 25 μM S-protein, 25 μM taxol, 1.9 μM actinomycin D, 25 μM RNase S, or 25 μM RNase A and then incubated for 48 h. The culture medium was replaced with TRIZOL reagent (500 μL, Thermo Fisher Scientific) and the cells were dissolved directly by pipetting. After incubating at 25 °C for 5 min, chloroform (100 μL) was added to the mixture, which was then shaken violently for 15 s and incubated at 25 °C for 3 min. The mixture was centrifuged at 12,000 g for 15 min at 4 °C, and then 2-propanol (250 μL) was added to the supernatant. After standing at 25 °C for 10 min, the mixture was centrifuged at 12,000 g for 10 min at 4 °C. After the supernatant was removed, the RNA pellet was obtained from the bottom. The RNA pellet was washed once with 75% ethanol aq. (1 mL, prepared with Ultrapure™ DNase/RNase-Free Distilled Water), vortexed, and centrifuged at 7500 g for 5 min at 4 °C. After the supernatant was removed, the pellet was air-dried for 5 min. Ultrapure™ DNase/RNase-Free Distilled Water (500 μL) was added to the resulting RNA pellet and incubated at 60 °C for 10 min to dissolve the RNA. The absorbance of each sample was measured using a NanoDrop™ One/OneC (ND-ONE–W, Thermo Fisher Scientific) at 260 nm. RNA quantity (%) was calculated by setting the absorbance of the untreated HepG2 cells at 100%.

Conflict of Interest

The authors declare no conflict of interest.

Data Availability Statement

Research data are not shared.

[1] R. Raines, *Chem. Rev.* **1998**, *98*, 1045–1066.
[2] A. Makarov, O. Ilinskaya, *FEBS Lett.* **2003**, *540*, 15–20.
[3] W. Ardelt, B. Ardelt, Z. Darzynkiewicz, *Eur. J. Pharmacol.* **2009**, *625*, 181–189.
[4] S. M. Rybak, M. A. E. Arndt, T. Schirrmann, S. Dubel, J. Krauss, *Curr. Pharm. Des.* **2009**, *15*, 2665–2675.
[5] C. Cobaleda, I. Sánchez-García, *Trends Biotechnol.* **2001**, *19*, 406–411.
[6] J. Matousek, G. Gotte, P. Pouckova, J. Soucek, T. Slavik, F. Vottariello, M. Libonati, *J. Biol. Chem.* **2003**, *278*, 23817–23822.
[7] J. Matoušek, *Comp. Biochem. Physiol. C Toxicol. Pharmacol.* **2001**, *129*, 175–191.
[8] G. Torrent, M. Ribó, A. Benito, M. Vilanova, *Mol. Pharmaceutics.* **2009**, *6*, 531–542.
[9] S. S. Kanwar, R. Kumar, *J. Mol. Catal. B* **2017**, *6*, 162.
[10] J. Castro, M. Ribó, M. Vilanova, A. Benito, *Pharmaceutica* **2021**, *13*, 82.
[11] J. Dubois, N. Lavignac, *J. Mater. Chem. B* **2015**, *3*, 6501–6508.
[12] T. Rutkosk, J. Kink, L. Strong, C. Schilling, R. Raines, *Bioconjugate Chem.* **2010**, *21*, 1691–1702.
[13] G. Gotte, M. Menegazzi, *Front. Immunol.* **2019**, *10*, 2626.
[14] M. Mastronicola, R. Piccoli, G. D'Alessio, *Eur. J. Biochem.* **1995**, *230*, 242–249.
[15] M. Iordanov, O. Ryabinina, J. Wong, T. Dinh, D. Newton, S. Rybak, B. Magun, *Cancer Res.* **2000**, *60*, 1983–1994.
[16] V. Mitkevich, O. Ilinskaya, A. Makarov, *Cell Cycle* **2015**, *14*, 931–932.
[17] D. Cernia, R. Sorrentino, S. Gaetano, A. Arciello, C. Garbi, R. Piccoli, G. D'Alessio, G. Vecchio, P. Laccetti, M. Santoro, *J. Clin. Endocrinol. Metab.* **2003**, *88*, 2900–2907.
[18] D. Spalletti-Cernia, R. Sorrentino, S. Gaetano, R. Piccoli, M. Santoro, G. D'Alessio, P. Laccetti, G. Vecchio, *Br. J. Cancer* **2004**, *90*, 270–277.
[19] D. Concolino, F. Deodato, R. Parini, *Ital. J. Pediatr.* **2018**, *44*, 120.
[20] F. Osaki, T. Kanamori, S. Sando, T. Sera, Y. Aoyama, *J. Am. Chem. Soc.* **2004**, *126*, 6520–6521.
[21] J. Wen, B. Kim, T. James, W. Chan, *Nat. Nanotechnol.* **2008**, *3*, 145–150.
[22] T. Maack, V. Johnson, S. Kau, J. Figueiredo, D. Sigulem, *Kidney Int.* **1979**, *16*, 251–270.
[23] K. Narayanan, S. Han, *Adv. Colloid Interface Sci.* **2017**, *248*, 1–19.
[24] S. Bode, I. Minten, R. Nolte, J. Cornelissen, *Nanoscale* **2011**, *3*, 2376–2389.
[25] M. Comellas-Aragonès, H. Engelkamp, V. Claessen, N. Sommerdijk, A. Rowan, P. Christianen, J. Maan, B. Verduin, J. Cornelissen, R. Nolte, *Nat. Nanotechnol.* **2007**, *2*, 635–639.
[26] L. Schoonen, S. Maassen, R. Nolte, J. Hest, *Biomacromolecules.* **2017**, *18*, 3492–3497.
[27] D. Patterson, P. Prevelige, T. Douglas, *ACS Nano* **2012**, *6*, 5000–5009.
[28] R. Feiner, J. Teschner, K. Teschner, M. Radukic, T. Baumann, S. Hagen, Y. Hannappel, N. Biere, D. Anselmetti, K. Arndt, K. Müller, *Int. J. Mol. Sci.* **2019**, *20*, 5702.
[29] S. Gleiter, K. Stubenrauch, H. Lilie, *Protein Sci.* **1999**, *8*, 2562–2569.
[30] M. Cayetano-Cruz, C. Coffeen, J. Valadez-García, C. Montiel, I. Bustos-Jaimes, *Virus Res.* **2018**, *255*, 1–9.
[31] A. Aljabali, J. Barclay, N. Steinmetz, G. Lomonossoff, D. Evans, *Nanoscale* **2012**, *4*, 5640–5645.
[32] S. Bhaskar, S. Lim, *NPG Asia Mater.* **2017**, *9*, e371.
[33] Y. Lai, E. Reading, G. Hura, K. Tsai, A. Laganowsky, F. Asturias, J. Tainer, C. Robinson, T. Yeates, *Nat. Chem.* **2014**, *6*, 1065–1071.
[34] L. Schoonen, J. Hest, *Nanoscale* **2014**, *6*, 7124–7141.
[35] A. Malay, N. Miyazaki, A. Biela, S. Chakraborti, K. Majsterkiewicz, I. Stupka, C. Kaplan, A. Kowalczyk, B. Piette, G. Hochberg, D. Wu, T.

Wrobel, A. Fineberg, M. Kushwah, M. Kelemen, P. Vavpetič, P. Pelicon, P. Kukura, J. Benesch, K. Iwasaki, J. Heddle, *Nature* **2019**, *569*, 438–422.

[36] K. Majsterkiewicz, Y. Azuma, J. Heddle, *Nanoscale Adv.* **2020**, *2*, 2255–2264.

[37] A. Cristie-David, J. Chen, D. Nowak, A. Bondy, K. Sun, S. Park, M. Holl, M. Su, E. Marsh, *J. Am. Chem. Soc.* **2019**, *141*, 9207–9216.

[38] N. Kawakami, H. Kondo, Y. Matsuzawa, K. Hayasaka, E. Nasu, K. Sasahara, R. Arai, K. Miyamoto, *Angew. Chem. Int. Ed.* **2018**, *57*, 12400–12404; *Angew. Chem.* **2018**, *130*, 12580–12584.

[39] B. Ramakers, J. Hest, D. Löwik, *Chem. Soc. Rev.* **2014**, *43*, 2743–2756.

[40] S. Lou, X. Wang, Z. Yu, L. Shi, *Adv. Sci.* **2019**, *6*, 1802043.

[41] J. Fletcher, R. Harniman, F. Barnes, A. Boyle, A. Collins, J. Mantell, T. Sharp, M. Antognozzi, P. Booth, N. Linden, M. Miles, R. Sessions, P. Verkade, D. Woolfson, *Science* **2013**, *340*, 595–599.

[42] M. Mosayebi, D. Shoemark, J. Fletcher, R. Sessions, N. Linden, D. Woolfson, T. Liverpool, *Proc. Natl. Acad. Sci. USA* **2017**, *114*, 9014–9019.

[43] E. Santis, H. Alkassem, B. Lamarre, N. Faruqui, A. Bella, J. Noble, N. Micale, S. Ray, J. Burns, A. Yon, B. Hoogenboom, M. Ryadnov, *Nat. Commun.* **2017**, *8*, 2263.

[44] I. Kepiro, I. Marzuoli, K. Hammond, X. Ba, H. Lewis, M. Shaw, S. Gunnoo, E. Santis, U. Łapińska, S. Pagliara, M. Holmes, C. Lorenz, B. Hoogenboom, F. Fraternali, M. Ryadnov, *ACS Nano.* **2020**, *14*, 1609–1622.

[45] Y. Lai, E. Reading, G. Hura, K. Tsai, A. Laganowsky, F. Asturias, J. Tainer, C. Robinson, T. Yeates, *Nat. Chem.* **2014**, *6*, 1065–1071.

[46] J. Bale, S. Gonen, Y. Liu, W. Shellfer, D. Ellis, C. Thomas, D. Cascio, T. Yeates, T. Gonen, N. King, D. Baker, *Science* **2016**, *353*, 389–394.

[47] Y. Hsia, J. Bale, S. Gonen, D. Shi, W. Sheffler, K. Fong, U. Nattermann, C. Xu, P. Huang, R. Ravichandran, S. Yi, T. Davis, T. Gonen, N. King, D. Baker, *Nature* **2016**, *535*, 136–139.

[48] K. Matsuura, K. Watanabe, T. Matsuzaki, K. Sakurai, N. Kimizuka, *Angew. Chem. Int. Ed.* **2010**, *49*, 9662–9665; *Angew. Chem.* **2010**, *122*, 9856–9859.

[49] K. Matsuura, *RSC Adv.* **2014**, *4*, 2942–2953.

[50] K. Matsuura, *Chem. Commun.* **2018**, *54*, 8944–8959.

[51] K. Matsuura, K. Watanabe, Y. Matsushita, N. Kimizuka, *Polym. J.* **2013**, *45*, 529–534.

[52] Y. Nakamura, H. Inaba, K. Matsuura, *Chem. Lett.* **2019**, *48*, 544–546.

[53] Y. Nakamura, Y. Sato, H. Inaba, T. Iwasaki, K. Matsuura, *Appl. Sci.* **2020**, *10*, 8004.

[54] K. Matsuura, T. Nakamura, K. Watanabe, T. Noguchi, K. Minamihata, N. Kamiya, N. Kimizuka, *Org. Biomol. Chem.* **2016**, *14*, 7869–7874.

[55] K. Sakamoto, H. Furukawa, J. Arafiles, M. Imanishi, K. Matsuura, S. Futaki, *Bioconjugate Chem.* **2022**, *33*, 311–320.

[56] K. Matsuura, G. Ueno, S. Fujita, *Polym. J.* **2015**, *47*, 146–151.

[57] K. Matsuura, T. Honjo, *Bioconjugate Chem.* **2019**, *30*, 1636–1641.

[58] K. Matsuura, Y. Shiomi, T. Mizuta, H. Inaba, *Processes* **2020**, *8*, 1455.

[59] I. Hamachi, J. Watanabe, R. Eboshi, T. Hiraoka, S. Shinkai, *Pept. Sci.* **2000**, *55*, 459–468.

[60] M. Bastings, T. Greef, J. Dongen, M. Merkx, E. Meijer, *Chem. Sci.* **2010**, *1*, 79–88.

[61] J. Kim, R. Raines, *Protein Sci.* **1993**, *2*, 348–256.

[62] W. Appel, E. Meijer, P. Dankers, *Macromol. Biosci.* **2011**, *11*, 1706–1712.

[63] M. Aubin, D. Morales, K. Hamad-Schifferli, *Nano Lett.* **2005**, *5*, 519–522.

[64] J. DiMaio, D. Raymond, B. Nilsson, *Org. Biomol. Chem.* **2017**, *15*, 5279–5283.

[65] B. Jankovic, A. Gulzar, C. Zanobini, O. Bozovic, S. Wolf, G. Stock, P. Hamm, *J. Am. Chem. Soc.* **2019**, *141*, 10702–10710.

[66] C. Grison, G. Burslem, J. Miles, L. Pilsl, D. Yeo, Z. Imani, S. Warriner, M. Webb, A. Wilson, *Chem. Sci.* **2017**, *8*, 5166–5171.

[67] K. Matsuura, J. Ota, S. Fujita, Y. Shiomi, H. Inaba, *J. Org. Chem.* **2020**, *85*, 1668–1673.

[68] E. Simons, E. Blout, *J. Biol. Chem.* **1968**, *243*, 218–221.

[69] D. Lu, Y. Wang, C. Li, G. Wei, R. Chen, D. Dong, M. Yao, *Int. J. Clin. Exp. Med.* **2015**, *8*, 1904–1911.

[70] T. Mosmann, *J. Immunol. Methods* **1983**, *65*, 55–63.